

TEMPERATURE BEHAVIOUR OF CERAMIC BIOCOMPOSITES INVESTIGATED VIA HOT-STAGE MICROSCOPY

JUSTYNA PAWLIK*, KATARZYNA CHOLEWA-KOWALSKA

AGH UNIVERSITY OF SCIENCE AND TECHNOLOGY,
FACULTY OF MATERIALS SCIENCE AND CERAMICS,
DEPARTMENT OF GLASS TECHNOLOGY AND
AMORPHOUS COATINGS,
AL. MICKIEWICZA 30, 30-059 KRAKOW, POLAND
*E-MAIL: PAWLIKJ@AGH.EDU.PL

Abstract

In this study, sol-gel bioactive glasses and β -TCP composites were investigated regarding their thermal behaviour, microstructure, and phase composition. Sol-gel bioactive glasses based on the CaO-SiO₂-P₂O₅ system of either a high SiO₂ content (S2) or a high CaO content (A2) were mixed with the β -TCP at 25:75, 50:50 and 75:25 weight ratios. Basing on the HSM results, i.e. shrinkage curves, densification intervals and characteristic temperatures, the sintering temperatures of composites were indicated. Scanning electron microscopy and X-ray diffraction were used to determine the microstructure and phase composition of composites after sintering at selected temperatures, i.e. 1100°C and 1200°C. The SEM/EDX investigations proved the well-sintered and densified microstructure of the sintered composites. The chemistry of sol-gel bioactive glasses influenced both the thermal behaviour and the phase composition of the composites. The dominant phases for A2- β -TCP materials were α -TCP, pseudowollastonite and β -TCP, while for S2- β -TCP – cristobalite, β -TCP, and α -TCP. However, the content of each phase varied, depending on the A2 or S2 content in the composite composition. Hot-stage microscopy provides useful information for selecting optimal sintering temperature in order to obtain well-sintered and strengthened material. Moreover, by a carefully selected combination of sol-gel bioactive glasses and β -TCP it is possible to obtain the materials with favorable phase composition with regard to biological activity.

Keywords: Hot-Stage Microscopy, sol-gel glasses, bioactive glasses, biocomposites, tricalcium phosphates, β -TCP, sintering

[Engineering of Biomaterials 150 (2019) 22-28]

Introduction

Bioceramic materials, such as bioactive glasses, hydroxyapatite or tricalcium phosphates, are widely investigated as synthetic bone grafts, due to their high biocompatibility and bone integration. Among them, bioactive sol-gel glasses prove enhancement of bioactive and biological properties, due to the presence of specific surface areas and higher solubility than the molten ones [1-3]. However, these materials have some limitations in terms of their physico-chemical properties, due to their deficient thermal behaviour impairing their sintering ability and mechanical performance [4,5]. To overcome these disadvantages bioactive glasses are often combined with other biomaterials like hydroxyapatite [5-7], titanium dioxide [8], polycaprolactone or other polymers [9-11]. The osteoconductive properties of calcium phosphates (i.e. hydroxyapatite, β - and α -tricalcium phosphates) have led to their use as a promising material for bone tissue repair. It is worth noticing that most of nowadays synthetic bone substitutes are composites of CaP's and/or another phase (PLA, bioglass, etc.). Several reports show that bioactive glass and HA composites exhibit stronger biological activities and enhanced mechanical performance in comparison to pure HA [12-14]. During the temperature treatment (upon 1000°C) hydroxyapatite may decompose into β -TCP and α -TCP. Both of them are recognized as biocompatible and more soluble than HA. In fact the solubility can be described as: HA < β -TCP < α -TCP [15,16].

The majority of ceramic biomaterials is fabricated by the thermal processing, mainly in order to obtain a desirable material shape and also to improve their mechanical properties thanks to the increase in crystallinity [17,18]. Studies reveal that high crystallinity of 45S5 Bioglass® may delay the surface activity, both *in vitro* and *in vivo* [19,20]. On the other hand, resistance to degradation and mechanical strength of bioactive glasses can be improved by the controlled crystallization of the material [21]. Physical and chemical phenomena occurring in ceramics materials during temperature treatment can be observed *in situ*, via the hot-stage microscopy (HSM). In general, this research method is based on investigating the sample placed inside the furnace, maintaining the necessary temperature and the thermal environment, while it is *in situ* observed with an optical instrument. A great variety of heating microscopes have been designed and used in materials science nowadays. The wide range of instrument specifications and the possibility of additional parameters measurements (i.e. simultaneous X-ray diffraction, differential calorimetric analyses, mapping of surface temperature distribution) give the great possibility and flexibility for the different specimen investigations [22,23].

There are three main components of the hot-stage microscope: 1) the electric furnace with the specimen carriage; 2) the observation unit with the microscope and the recording device (video camera); 3) the light source. The scheme of the HSM used in this work is presented in FIG. 1.

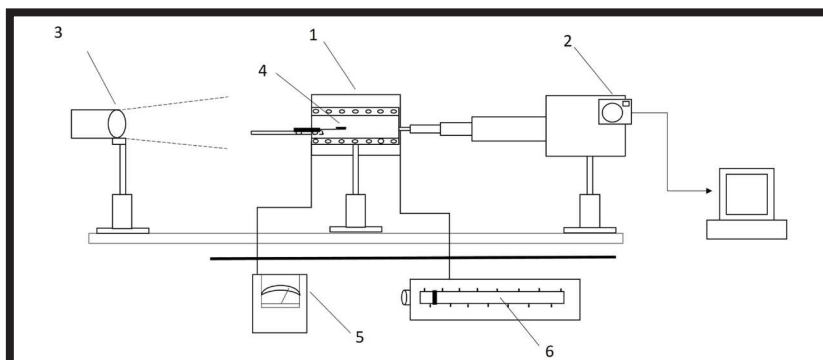


FIG. 1. Scheme of the hot-stage microscope:

- 1 - electric furnace,
- 2 - observation unit with the image/video recording,
- 3 - light source,
- 4 - specimen and thermocouple,
- 5 - temperature controller,
- 6 - heating device.

The results of HSM investigations define the thermal behaviour of samples thanks to the specification of characteristic temperature values [23-25]:

- T_s - initial shrinkage temperature – when the melting begins on the contact points of the particular grains, while simultaneously the specimen size diminishes, but without changes of the initial shape,
- T_{sf} - softening temperature – when the first symptom of the specimen softening occurs with the visible shape changes, i.e. rounding off the cylinder corners of the specimen,
- T_m - melting temperature – when the specimen is melting, assuming the hemispherical form (generally established when hemisphere height equals approximately 2/3 of the initial specimen height),
- T_f - flowing temperature – when the specimen is flowing and forming a layer whose thickness is approximately equal to 1/3 of the specimen initial height.

The HSM results provide valuable data concerning not only the characteristic temperature values of the material (i.e. sintering softening, melting and flowing) but also its viscosity, wettability and surface tension [26-28]. This method is appropriate for examinations of glass, slags, ceramics, glazes and various raw materials by *real-time* observation and recording (photo capture or video record) how the sample contours change during the temperature increase [24]. Moreover, the most recent reports have proved that HSM is an effective method to investigate the thermal behaviour of biomaterials [29,30]. Hot stage microscopy was used to investigate new kinds of bioactive glass [29,31,32], bioglasses-based scaffolds [33,34] and ceramic-based biomaterials [35,36] in order to estimate their sintering ability. The usefulness of this method was proved in defining sintering routines and it stays in agreement with our previous investigations [5,37,38]. It is evident that a satisfactory balance of the biomaterial porosity/density and its mechanical strength is a key factor for biomaterials fabricated via thermal methods, as it affects their final physico-chemical properties and biological activity.

In this paper, we propose the application of the hot-stage microscopy to investigate biocomposites combined with the sol-gel bioactive glass (SBG) and β -TCP. These composites are intended as biomedical devices. We show here the practical use of HSM by examining composition of different composites (i.e. chemical composition of bioglass A2 - high lime glass, S2 - high silica glass and 25-75wt% of glass content in the composite) in order to evaluate their sintering temperatures necessary for materials processing. The major advantage of hot-stage microscopy is the possibility to determine the characteristic temperatures and thermal properties at the very early stage of the biomaterials designing, thus evaluating their usefulness. Further, in our work we present the results of composites sintered at selected temperatures along with the evaluation of their microstructure (SEM/EDX) and phase composition (XRD).

Materials and Methods

Two types of sol-gel bioactive glass (SBG) derived from the SiO_2 -CaO- P_2O_5 system were synthesized as described previously [39,40]. They differed in chemical compositions and were designed as A2: 40 SiO_2 -54CaO-6 P_2O_5 [%mol.] and S2: 80 SiO_2 -16CaO-4 P_2O_5 [%mol.]. Summing up the process briefly, tetraethoxysilane (TEOS: $\text{Si}(\text{OC}_2\text{H}_5)_4$), triethylphosphate (TEP: $\text{OP}(\text{OC}_2\text{H}_5)_3$) and calcium nitrate tetra-hydrate ($\text{Ca}(\text{NO}_3)_2 \cdot 4\text{H}_2\text{O}$) were used as starting components in the sol-gel process.

HCl solution was used as a catalyst for the hydrolysis and condensation reactions. The formed gel was dried in the oven at 800°C for 20 h and then milled and sieved to obtain a bioactive glass powder with particle sizes <45 μm .

Calcium phosphate – β TCP, purity $\geq 96.0\%$ (CAS 7758-87-4) was purchased from Sigma-Aldrich, Germany.

Two types of sol-gel bioactive glass - S2 or A2 - were used to fabricate composites with β -TCP in the weight ratio of 25:75, 50:50 and 75:25. Pure A2, S2, and β -TCP materials were used as reference samples. Mixed and homogenized powders were used to prepare pellets (of 10 mm diameter) by uniaxial pressure at 100 MPa. Based on the HSM results - depending on the composites composition - the sintering temperature was 1100°C (S2- β TCP and the reference materials: S2, β TCP) or 1200°C (A2- β TCP and the reference sample A2). The heating rate was 5°C/min and the samples were held at the sintering temperature for 2 h and then cooled inside the furnace.

Hot-stage microscopy

The temperature behaviour and sintering ability of the SBG- β -TCP samples and reference ones were investigated by the hot-stage microscope (Leitz Wetzlar, Germany). The tests were performed in air using a heating rate schedule of 10°C/min between the 20°C and 1400°C. The mixed and homogenized powders were manually pressed into a cylindrical shape (3 x 3 mm). The compacted sample placed on the ceramic holder was inserted into the furnace at the room temperature and then the heating process started. The test proceeded until the temperature reached 1400°C or the flowing temperature of the sample was reached. While being heated the samples were observed with the video camera (magnification 20x) and thus the images of the changing sample profiles were acquired (FIG. 2). The potential systematic error occurrence was minimized by analyzing 3 samples of each material. Therefore, presented herein results of HM were described as mean \pm standard deviation. The sample shrinkage at different temperatures (TABLE 1, FIG. 2) was calculated from the variation of the sample area, applying the following formula:

$$\text{Shrinkage (\%)} = (A_T/A_0) \times 100$$

where:

A_T – area of the sample at the temperature T [mm^2],

A_0 – initial area of the sample at room temperature [mm^2].

Scanning electron microscopy

The scanning electron microscopy (SEM) and energy dispersive X-ray analysis (EDX) (NOVA 200, NanoSEM, FEI, USA) were used to characterize the microstructure of the samples sintered at selected temperatures, i.e. 1100°C and 1200°C. The samples were sputtered with a thin layer of carbon and images were taken (mag. 1000x) at an operation voltage of 18 kV. The presented results are representative for each sample, yet several SEM/EDX analyses of different areas of each material were performed (FIG. 4).

X-ray diffraction

The phase composition of the heat-treated samples was studied by X-ray diffraction analysis (Philips X'Pert Pro MD) and the XRD patterns of the SBG- β -TCP composites and the reference materials are presented in FIG. 5. The phase identification was carried out by means of the PANalytical X'Pert HighScore Plus software.

Results and Discussions

Hot-stage microscopy was used to evaluate the thermal behaviour of SBG- β -TCP composites and reference samples (S2, A2, and β -TCP). The variations of samples shrinkage depending on the temperature are showed in FIG. 2. The thermal behaviour of composites followed the multi-stage shrinkage (densification) process characteristic for composite materials. However, the temperatures of each stage of densification varied depending on the composites composition and mostly were characterized by the temperature interval T_1 - T_2 and T_3 - T_4 (FIG. 2). Generally, the A2 glass samples were more thermally stable and the first stage of densification for the A2- β -TCP composites ranging from 1100-1270°C, while for the S2- β -TCP materials the first shrinkage temperature varied from 980-1150°C. The second stage of densification for the S2 glass composites was observed between 1110-1200°C. However, with the increasing temperature, the dimensions of the S2- β -TCP samples remained unchanged until the end of the test and the plateau of shrinkage curves for these samples was observed.

This observation corresponds to the thermal curve for pure S2-sample. However, in this case, the only shrinking occurred at the lower temperature (780-800°C) and, despite heating, the material maintained its unchanged dimensions (plateau). This phenomenon can be correlated with the crystallization process when the viscosity increases and the viscous flow sintering is inhibited. For the A2 composites the temperature values of the second shrinkage stage were higher when compared to the S2- β -TCP samples, from 1280-1350°C. Moreover, with the increase in temperature, the samples dimensions decreased continuously. This may be attributed to the rapid reduction of the samples shape caused by increased softness and rapid decrease in viscosity, probably resulting from sintering with the liquid phase. The greatest shrinkage was observed for the A2- β -TCP composites (62-75%), while the S2- β -TCP composite revealed the shrinkage range from 82 to 94% (TABLE 1). These differences correlate with the type of glass (A2 or S2) in the composite composition, with the shrinkage of 64% and 86%, respectively.

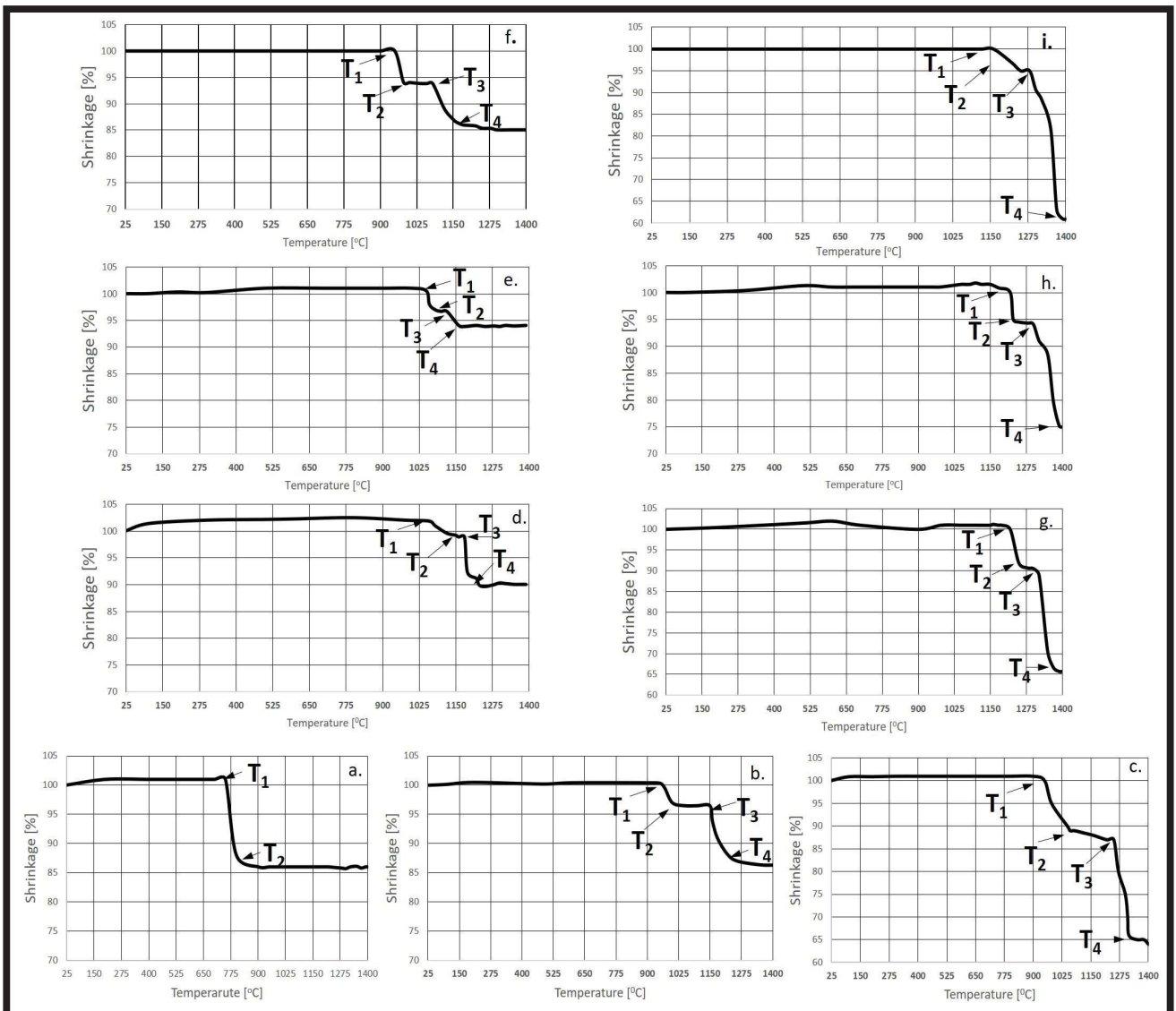


FIG. 2. Shrinkage curves derived from the HSM as a function of temperature for SBG- β -TCP composites and reference materials. Where: a. - S2, b. - β -TCP, c. - A2, d. - 25S2- β -TCP, e. - 50S2- β -TCP, f. - 75S2- β -TCP, g. - 25A2- β -TCP, h. - 50A2- β -TCP, i. - 75A2- β -TCP.

T_1 , T_2 - temperature at the beginning and the end of the first densification stage,
 T_3 , T_4 - temperatures at the beginning and the end of the second densification stage.

TABLE 1. Characteristics of SBG-β-TCP composites and reference materials (A2, S2, β-TCP).

Sample	Shrinkage* [%]	Densification intervals* [°C]		Sintering temperature [°C]	Apparent density** [g/cm³]
		T ₁ -T ₂	T ₃ -T ₄		
25A2-β-TCP	65.1 ± 0.2	1270-1300°C (ΔT = 30)	1350-1370°C (ΔT = 20)	1200	2.01 ± 0.12
50A2-β-TCP	75.0 ± 1.2	1230-1280°C (ΔT = 50)	1320-1390°C (ΔT = 70)	1200	1.69 ± 0.05
75A2-β-TCP	62.2 ± 0.3	1210-1250°C (ΔT = 40)	1310-1370°C (ΔT = 60)	1200	1.61 ± 0.07
25S2-β-TCP	90.1 ± 0.2	1120-1160°C (ΔT = 40)	1200-1280°C (ΔT = 80)	1100	2.46 ± 0.04
50S2-β-TCP	94.5 ± 1.1	1060-1100°C (ΔT = 40)	1160-1210°C (ΔT = 50)	1100	2.03 ± 0.06
75S2-β-TCP	82.1 ± 0.4	980-1020°C (ΔT = 40)	1120-1160°C (ΔT = 40)	1100	1.74 ± 0.02
A2	64.3 ± 0.5	980-1050°C (ΔT = 25)	1260-1310°C (ΔT = 50)	1200	1.71 ± 0.04
S2	86.0 ± 0.2	780-850°C (ΔT = 70)	-	1100	1.55 ± 0.03
β-TCP	86.3 ± 0.2	970-1050°C (ΔT = 80)	1180-1220°C (ΔT = 40)	1100	2.23 ± 0.10

* based on the hot-stage microscopy results

** apparent density of samples after sintering at the selected temperature

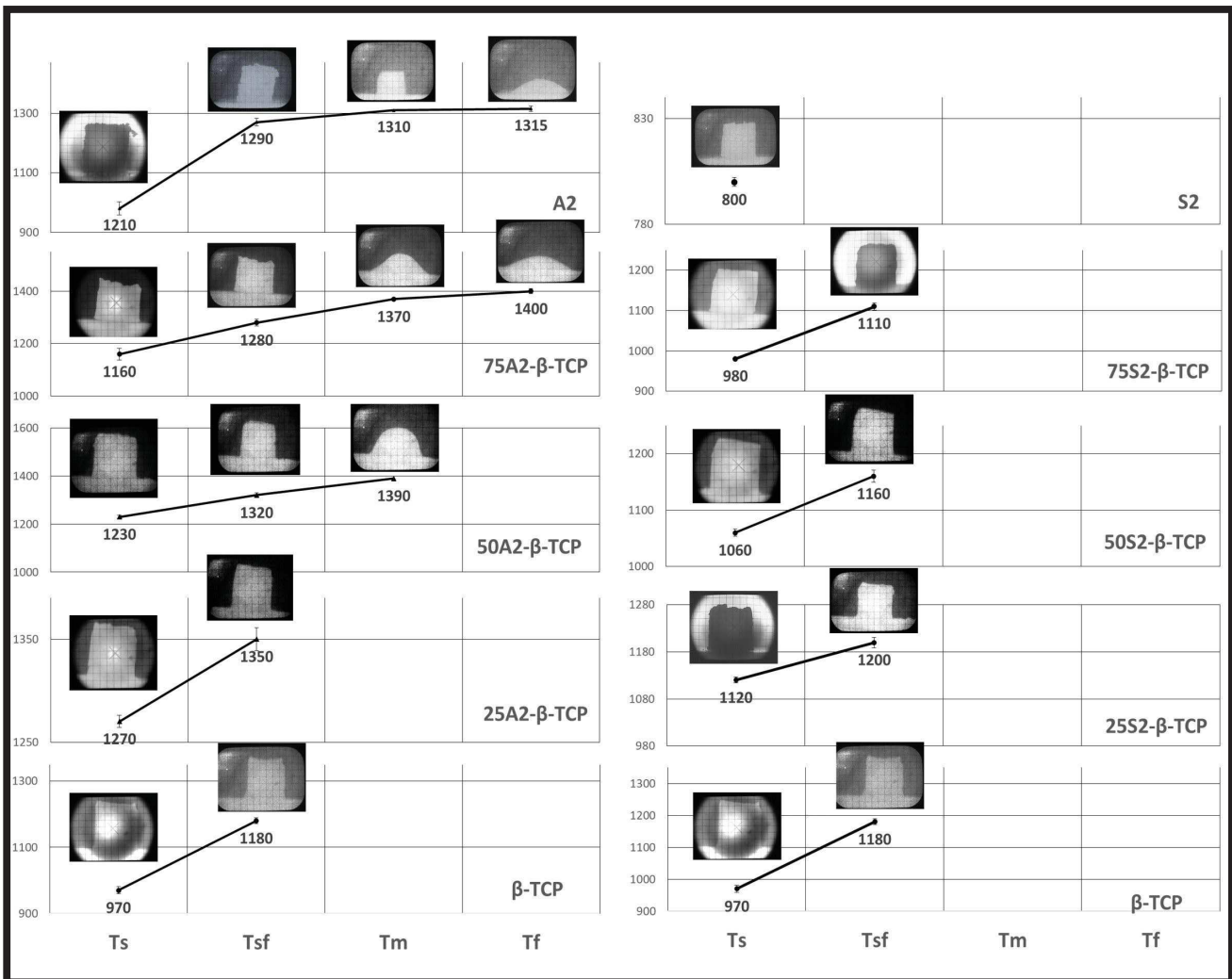


FIG. 3. The characteristic temperatures with correlated HTM images for A2-β-TCP, S2-β-TCP composites and reference sample (β-TCP, A2, S2). Where: T_s - initial shrinkage temperature, T_{sf} - softening temperature, T_m - melting temperature, T_f - flowing temperature.

Selecting the sintering temperatures of composites is a key step during the fabrication process. The hot-stage microscopy provides useful information how to accomplish this task. Basing on the shrinkage curves, the densification intervals and the *in situ* observation during HSM measurements the characteristic temperatures (i.e. T_s - initial shrinkage temperature, T_{sf} - softening temperature, T_m - melting temperature, T_f - flowing temperature) of the materials were selected. The results are presented in FIG. 3. A significant correspondence between the values of characteristic temperatures and the composition of composites can be observed:

- The addition of β -TCP to the composite composition influenced the increase in the characteristic temperatures in comparison with the addition of glass A2 or S2.
- The type of bioactive glass, i.e. A2 or S2, determines the values of characteristic temperatures, thus A2- β -TCP composites presented generally higher T_s and T_{st} than the S2- β -TCP materials.
- Both types of composites, i.e. A2- β -TCP and S2- β -TCP, showed the decrease in characteristic temperatures values with the increasing bioactive glass content.

- Only for the composites with 50 and 75wt% of A2 glass addition, the melting temperatures were visible, and the latter also revealed the flowing temperature, while negligible changes of the sample dimensions were observed for other materials beyond the sintering temperature.

As mentioned before, the results of hot-stage microscopy tests and *in-situ* observations of the sample profile during the measurements provide useful information for selecting the optimal sintering temperature to fabricate ceramic composites. This is a key parameter for obtaining the well densified and thus strengthened material with high biological activity provided by means of the phase composition. Therefore, the sintering temperatures for such glass-ceramic composites are usually considered between the T_s (initial shrinkage temperature) and T_{sf} (softening temperature). Based on the results of hot stage microscopy, the sintering temperatures of the SBG- β -TCP and the reference materials were selected as follows: 1100°C (β -TCP, S2, S2- β -TCP) and 1200°C (A2, A2- β -TCP) (TABLE 1).

The microstructure of the sintered SBG- β -TCP composites investigated by the SEM/EDX is presented in FIG. 4.

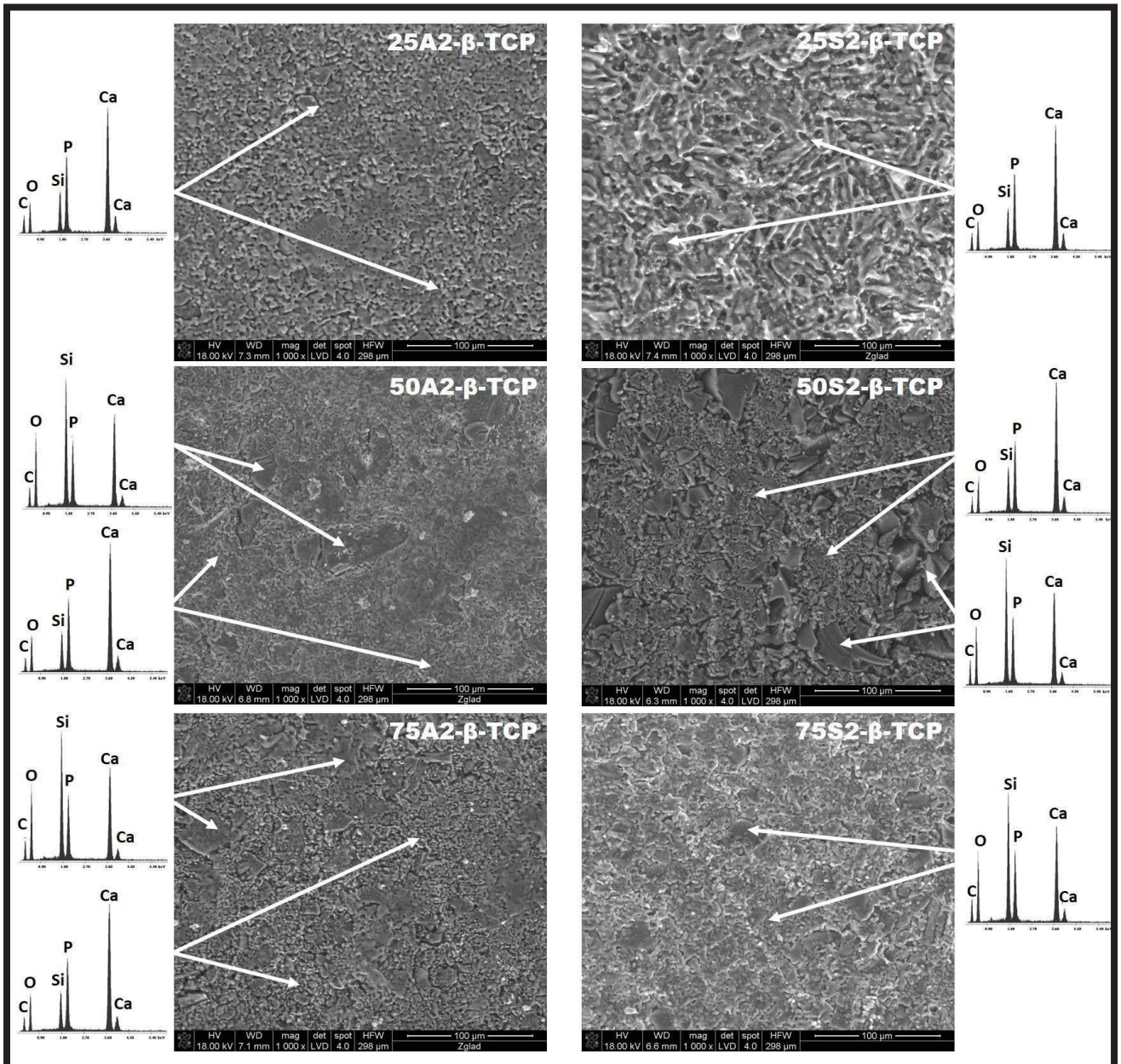


FIG. 4. SEM pictures and EDX spectra of SBG- β -TCP composites.

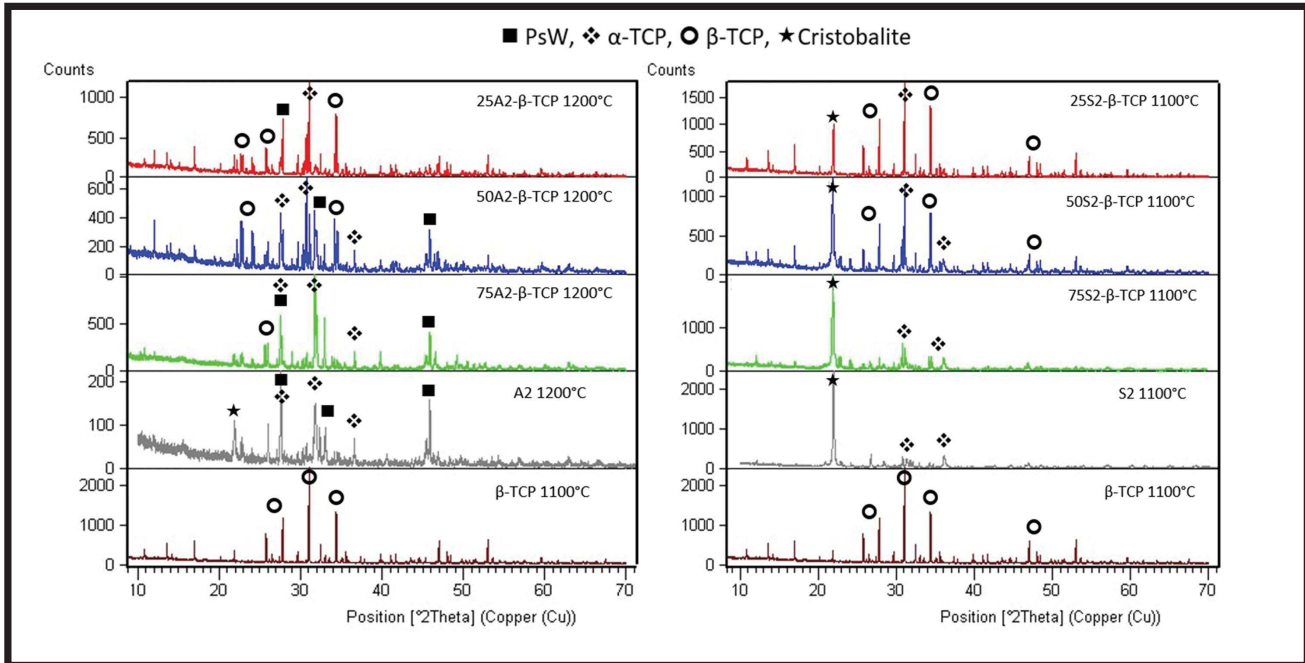


FIG. 5. XRD patterns of A2- β -TCP, S2- β -TCP composites and reference materials.

The composites with 25wt% of either S2 or A2 were homogeneously sintered materials, which was also confirmed by the EDX analysis. In the case of the 50A2- β -TCP samples and the 50S2- β -TCP ones the weaker integration of glass particles in the β -TCP matrix was observed. These composites also showed the less uniform microstructure in comparison with other materials. With the increasing content of glass in the composite composition (75A2- β -TCP and 75S2- β -TCP) the more homogenous microstructure with uniformly distributed and well-integrated β -TCP particles in the glass matrix was presented. However, in the case of the 75A2- β -TCP materials the domains enriched with Si or Ca and P were reported by the EDX analysis. Nevertheless, the sintering process led to the smoothness of glass particles which were no longer distinguishable.

The XRD plots of the SBG- β -TCP composites and the reference materials sintered at 1100°C or 1200°C and then ground into powder for diffraction analysis are reported in FIG. 5. The reference samples were represented by the following phases: S2 – cristobalite (70.8%) and α -TCP (29.2%), A2 – pseudowollastonite PsW (66.9%), α -TCP (20.3%) and cristobalite (12.8%). The phase composition of β -TCP after sintering at 1100°C remained unchanged. The XRD analyses indicated that α -TCP, pseudowollastonite and β -TCP were the main phases of the A2- β -TCP composites. However, the content of each phase varied, depending on the content of A2 in the composite. Thus, the dominant phases for 25A2- β -TCP were β -TCP (62.3%) and α -TCP (27.2%), while for the 75A2- β -TCP – PsW (42.3%) and α -TCP (40.9%). The main phases for the S2- β -TCP composites were cristobalite, β -TCP and α -TCP. Similarly, as in the case of A2- β -TCP, the amount of S2 glass in the composite influenced its phase composition. The dominant phase for the 25S2- β -TCP materials were β -TCP (47.2%) and α -TCP (28.7%), while for the 75S2- β -TCP only two phases existed after sintering – cristobalite (54.5%) and α -TCP (45.5%). The results of XRD analyses indicated the strong correlation between the chemical composition of sol-gel glasses (A2 and S2) and the phase composition of the samples. It can be concluded that introduction of either A2 or S2 affected the β -TCP \rightarrow α -TCP transformation, especially in the case of the 75S2- β -TCP materials.

The alteration of the transition temperature of β -TCP to α -TCP by the Si presence has also been reported by other authors [41,42]. Finally, the increased content of α -TCP in the phase composition of composites can be considered as beneficial when considering the bioactive behaviour of materials.

Conclusions

In this work, we investigated the temperature behaviour, phase composition and microstructure of sol-gel bioactive glasses and β -TCP composites. The type of glass used as a composite addition strongly affected the shrinkage profile and the values of characteristic temperatures established upon hot-stage microscopy analyses. Based on these studies the sintering temperatures for the composites and the reference materials were established between the T_s and T_{st} – between the first and second stage of densification. Thus, the composites and the reference materials were sintered as follows: 1100°C (S2, β -TCP, S2- β -TCP) and 1200°C (A2, A2- β -TCP). The SEM/EDX analyses showed the well-sintered and densified microstructure of composites. However, the 25(A2/S2)- β -TCP and the 75(A2-S2)- β -TCP materials proved acceptable homogeneity with the uniformly distributed and well-integrated both constituents. The chemical composition of sol-gel glass clearly influenced the phase composition of composites, but both A2- β -TCP and S2- β -TCP showed the presence of TCP (i.e. α -TCP and β -TCP) – the resorbable phase of high bioactivity and biocompatibility as the dominating one. In conclusion, our results indicate that both SBG- β -TCP composites may be an interesting candidates for biomaterials, however further investigations on mechanical strength, bioactivity or biological activity are needed.

Acknowledgments

This work was supported by the Ministry of Science and Higher Education, grant no 16.16.160.557. We are especially grateful for helpful commitment in HSM measurements by M.Sc. Tomasz Kawala and M.Sc. Justyna Smoleń.

References

- [1] J.R. Jones, A. Clare: Bio-glasses: an introduction, Wiley, 2012.
- [2] J.R. Jones, L.M. Ehrenfried, L.L. Hench: Optimising bioactive glass scaffolds for bone tissue engineering. *Biomaterials* 27 (2006) 964–973. doi:10.1016/J.BIOMATERIALS.2005.07.017.
- [3] F. Baino, E. Fiume, M. Miola, E. Verné: Bioactive sol-gel glasses: Processing, properties, and applications. *Int. J. Appl. Ceram. Technol.* 15 (2018) 841–860. doi:10.1111/ijac.12873.
- [4] Q.Z. Chen, I.D. Thompson, A.R. Boccaccini: 45S5 Bioglass®-derived glass-ceramic scaffolds for bone tissue engineering. *Biomaterials* 27 (2006) 2414–2425. doi:10.1016/j.biomaterials.2005.11.025.
- [5] K. Cholewa-Kowalska, J. Kokoszka, M. Łączka, et al.: Gel-derived bioglass as a compound of hydroxyapatite composites. *Biomed. Mater.* 4 (2009) 055007. doi:10.1088/1748-6041/4/5/055007.
- [6] D. Bellucci, A. Sola, V. Cannillo: Hydroxyapatite and tricalcium phosphate composites with bioactive glass as second phase: State of the art and current applications. *J. Biomed. Mater. Res. Part A.* 104 (2016) 1030–1056. doi:10.1002/jbm.a.35619.
- [7] G. Georgiou, J.C. Knowles: Glass reinforced hydroxyapatite for hard tissue surgery - Part 1: mechanical properties. *Biomaterials* 22 (2001) 2811–2815. doi:10.1016/S0142-9612(01)00025-4.
- [8] J. Pawlik, M. Ziąbka, R. Lach, M. Łączka, K. Cholewa-Kowalska: Tailoring the porosity, mechanical and bioactive properties of sol-gel bioactive glasses, hydroxyapatite and titanium dioxide porous composites. *J. Mech. Behav. Biomed. Mater.* 87 (2018) 40–49. doi:10.1016/J.JMBM.2018.07.012.
- [9] M. Dziadek, B. Zagrajczuk, E. Menaszek, K. Cholewa-Kowalska: A new insight into in vitro behaviour of poly(ϵ -caprolactone)/bioactive glass composites in biologically related fluids. *J. Mater. Sci.* 53 (2018) 3939–3958. doi:10.1007/s10853-017-1839-2.
- [10] P. Gentile, M. Mattioli-Belmonte, V. Chiono, et al.: Bioactive glass/polymer composite scaffolds mimicking bone tissue, *J. Biomed. Mater. Res. Part A.* 100A (2012) 2654–2667. doi:10.1002/jbm.a.34205.
- [11] J. Filipowska, J. Pawlik, K. Cholewa-Kowalska, G. Tylko, E. Pamula, L. Niedzwiedzki, et al.: Incorporation of sol-gel bioactive glass into PLGA improves mechanical properties and bioactivity of composite scaffolds and results in their osteoinductive properties. *Biomed. Mater.* 9 (2014). doi:10.1088/1748-6041/9/6/065001.
- [12] R. Ravarian, F. Moztafzadeh, M.S. Hashjin, S.M. Rabiee, P. Khoshakhlagh, M. Tahiri: Synthesis, characterization and bioactivity investigation of bioglass/hydroxyapatite composite. *Ceram. Int.* 36 (2010) 291–297. doi:10.1016/J.CERAMINT.2009.09.016.
- [13] S. Padilla, J. Román, S. Sánchez-Salcedo, M. Vallet-Regí: Hydroxyapatite/SiO₂-CaO-P₂O₅ glass materials: In vitro bioactivity and biocompatibility. *Acta Biomater.* 2 (2006) 331–342. doi:10.1016/J.ACTBIO.2006.01.006.
- [14] D. Bellucci, A. Sola, A. Anesi, R. Salvatori, L. Chiarini, V. Cannillo: Bioactive glass/hydroxyapatite composites: Mechanical properties and biological evaluation. *Mater. Sci. Eng. C.* 51 (2015) 196–205. doi:10.1016/J.MSEC.2015.02.041.
- [15] M. Bohner: Calcium orthophosphates in medicine: from ceramics to calcium phosphate cements. *Injury* 31(4) (2000) 37–47. <http://www.ncbi.nlm.nih.gov/pubmed/11270080>
- [16] W. Habraken, P. Habibovic, M. Epple, M. Bohner: Calcium phosphates in biomedical applications: materials for the future? *Mater. Today* 19 (2016) 69–87. doi:10.1016/J.MATTOD.2015.10.008.
- [17] J.B. Park: Bioceramics: properties, characterizations, and applications, Springer, 2008.
- [18] P.K. Chu, X. Liu: Biomaterials fabrication and processing handbook, CRC Press/Taylor & Francis, 2008.
- [19] O.P. Filho, G.P. La Torre, L.L. Hench: Effect of crystallization on apatite-layer formation of bioactive glass 45S5. *J. Biomed. Mater. Res.* 30 (1996) 509–514. doi:10.1002/(SICI)1097-4636(199604)30:4<509::AID-JBM9>3.0.CO;2-T.
- [20] R. Xin, Q. Zhang, J. Chen, Y. Leng: Effects of porosity and crystallinity of glass ceramics on the *in vivo* bioactive response. *Biomed. Mater.* 3 (2008) 041001. doi:10.1088/1748-6041/3/4/041001.
- [21] M. Plewinski, K. Schickle, et al.: The effect of crystallization of bioactive bioglass 45S5 on apatite formation and degradation. *Dent. Mater.* 29 (2013) 1256–1264. doi:10.1016/J.DENTAL.2013.09.016.
- [22] H.-J. Ullrich, R.W. Cahn, P. Haasen, E.J. Kramer (Eds). *Materials science and technology A comprehensive treatment. Vol. 2B: Characterization of Materials (Part II)* Volume Editor: E. Lifshin. VCH Weinheim; New York; Basel; Cambridge; Tokyo 1994 doi:10.1002/crat.2170290603.
- [23] S. (Severin) Amelinckx, *Handbook of microscopy: applications in materials science, solid-state physics, and chemistry*, VCH, 1997.
- [24] A.R. Boccaccini, B. Hamann: Review In Situ high-temperature optical microscopy, *J. Mater. Sci.* 34 (1999) 5419–5436. doi:10.1023/A:1004706922530.
- [25] H. Scholze: Influence of viscosity and surface tension on hot-stage microscopy measurements on glasses, *Ber. Dtsch. Keram. Ges.* 39 (1962) 63–68.
- [26] M. Garcia-Valles, H.S. Hafez, I. Cruz-Matías, E. Vergés, M.H. Aly, J. Nogués, D. Ayala, S. Martínez: Calculation of viscosity-temperature curves for glass obtained from four wastewater treatment plants in Egypt, *J. Therm. Anal. Calorim.* 111 (2013) 107–114. doi:10.1007/s10973-012-2232-7.
- [27] H. Scholze: Influence of viscosity and surface tension on hot-stage microscopy measurements on glasses. *Ver. Dtsch. Keramische Gesellschaft.* 391 (1962) 63–8.
- [28] R.L. Dumitrache, I. Teoreanu: Melting behaviour of feldspar porcelain glazes. *UPB Sci. Bull. Ser. B Chem. Mater. Sci.* 68 (2006) 3–16.
- [29] E. Mancuso, O.A. Bretcanu, M. Marshall, M.A. Birch, et al.: Novel bioglasses for bone tissue repair and regeneration: Effect of glass design on sintering ability, ion release and biocompatibility, *Mater. Des.* 129 (2017) 239–248. doi:10.1016/J.MATDES.2017.05.037.
- [30] S.S. Chon, L. Piraino, S. Mokhtari, E.A. Krull, A. Coughlan, Y. Gong, et al.: Synthesis, characterization and solubility analysis of amorphous SiO₂-CaO-Na₂O-P₂O₅ scaffolds for hard tissue repair, *J. Non. Cryst. Solids.* 490 (2018) 1–12. doi:10.1016/j.jnoncrysol.2018.03.006.
- [31] F. Baino, E. Fiume, M. Miola, F. Leone, B. Onida, F. Laviano, R. Gerbaldo, E. Verné: Fe-Doped Sol-Gel Glasses and Glass-Ceramics for Magnetic Hyperthermia. *Mater. (Basel, Switzerland).* 11 (2018). doi:10.3390/ma11010173.
- [32] M. Araújo, M. Miola, G. Baldi, J. Perez, E. Verné: Bioactive Glasses with Low Ca/P Ratio and Enhanced Bioactivity. *Mater. (Basel, Switzerland).* 9 (2016). doi:10.3390/ma9040226.
- [33] F. Baino, M. Ferraris, O. Bretcanu, E. Verné, C. Vitale-Brovarone: Optimization of composition, structure and mechanical strength of bioactive 3-D glass-ceramic scaffolds for bone substitution. *J. Biomater. Appl.* 27 (2013) 872–890. doi:10.1177/0885328211429193.
- [34] A.W. Wren, A. Coughlan, K.E. Smale, S.T. Misture, B.P. Mahon, O.M. Clarkin, M.R. Towler: Fabrication of CaO-NaO-SiO₂/TiO₂ scaffolds for surgical applications, *J. Mater. Sci. Mater. Med.* 23 (2012) 2881–2891. doi:10.1007/s10856-012-4746-8.
- [35] J. Vecstaudza, M. Gasik, J. Locs: Amorphous calcium phosphate materials: Formation, structure and thermal behaviour. *J. Eur. Ceram. Soc.* 39 (2019) 1642–1649. doi:10.1016/J.JEUR-CERAMSOC.2018.11.003.
- [36] V.O. Soares, J.K.M.B. Daguano, C.B. Lombello, O.S. Bianchin, L.M.G. Gonçalves, E.D. Zanotto: New sintered wollastonite glass-ceramic for biomedical applications, *Ceram. Int.* 44 (2018) 20019–20027. doi:10.1016/J.CERAMINT.2018.07.275.
- [37] J. Pawlik, M. Ziąbka, R. Lach, M. Łączka, K. Cholewa-Kowalska: Tailoring the porosity, mechanical and bioactive properties of sol-gel bioactive glasses, hydroxyapatite and titanium dioxide porous composites. *J. Mech. Behav. Biomed. Mater.* 87 (2018) 40–49. doi:10.1016/j.jmbm.2018.07.012.
- [38] J. Pawlik, M. Widziółek, K. Cholewa-Kowalska, M. Łączka, A.M. Osyczka: New sol-gel bioactive glass and titania composites with enhanced physico-chemical and biological properties. *J. Biomed. Mater. Res. - Part A.* 102 (2014). doi:10.1002/jbm.a.34903.
- [39] M. Łączka, K. Cholewa, A. Łączka-Osyczka: Gel-derived powders of CaO-P₂O₅-SiO₂ system as a starting material to production of bioactive ceramics. *J. Alloys Compd.* 248 (1997) 42–51. doi:10.1016/S0925-8388(96)02648-5.
- [40] M. Łączka, K. Cholewa-Kowalska, K. Kulgawczyk, M. Klisch, W. Mozgawa: Structural examinations of gel-derived materials of the CaO-P₂O₅-SiO₂ system. *J. Mol. Struct.* 511–512 (1999) 223–231. doi:10.1016/S0022-2860(99)00163-5.
- [41] A.M. Pietak, J.W. Reid, M.J. Stott, M. Sayer: Silicon substitution in the calcium phosphate bioceramics, *Biomaterials.* 28 (2007) 4023–4032. doi:10.1016/J.BIOMATERIALS.2007.05.003.
- [42] J. Duncan, S. Hayakawa, A. Osaka, J.F. MacDonald, J.V. Hanna, J.M.S. Skakle, I.R. Gibson: Furthering the understanding of silicate-substitution in α -tricalcium phosphate: An X-ray diffraction, X-ray fluorescence and solid-state nuclear magnetic resonance study, *Acta Biomater.* 10 (2014) 1443–1450. doi:10.1016/j.actbio.2013.11.014.